arXiv:1403.7195v1 [astro-ph.EP] 27 Mar 2014

The Gemini NICI Planet-Finding Campaign: The Orbit of the Young Exoplanet β Pictoris b

Eric L. Nielsen,[1] Michael C. Liu,[1] Zahed Wahhaj,[2] Beth A. Biller,[3] Thomas L. Hayward,[4] Jared R. Males,[5] Laird M. Close,[5] Katie M. Morzinski, [5] Andrew J. Skemer,[5] Marc J. Kuchner,[6] Mark Chun,[1] Christ Ftaclas,[1] Douglas W. Toomey[7]

ABSTRACT

We present new astrometry for the young (12–21 Myr) exoplanet β Pictoris b taken with the Gemini/NICI, Magellan/MagAO+Clio2, and Magellan/MagAO+VisAO instruments between 2009 and 2012. The high dynamic range of our observations allows us to measure the relative position of β Pic b with respect to its primary star with greater accuracy than previous observations. Based on a Markov Chain Monte Carlo analysis, we find the planet has an orbital semi-major axis of $9.2^{+8.3}_{-0.5}$ AU and orbital eccentricity < 0.15 at 68% confidence (with 95% confidence intervals of 8.2–72.3 AU and 0.00–0.88 for semi-major axis and eccentricity, respectively). We find that the planet has reached its maximum projected elongation, enabling higher precision determination of the orbital parameters than previously possible, and that the planet's projected separation is currently decreasing. With unsaturated data of the entire β Pic system (primary star, planet, and disk) obtained thanks to NICI's semi-transparent focal plane mask, we are able to tightly constrain the relative orientation of the circumstellar components. We find the orbital plane of the planet lies between the inner and outer disks but closer to the inner (warped) disk: the position angle (PA) of nodes (211.8±0.3°) is 6σ greater than the PA of the spine of the outer disk and 1.8σ less than the warped inner disk PA. Finally, for the first time we are able to dynamically constrain the mass of the primary star β Pic to 1.7±0.3 $M_\odot$.

Subject headings: planets and satellites: detection — stars: individual (β Pic) — planetary systems — planet-disk interactions

[1]Institute for Astronomy, University of Hawaii, 2680 Woodlawn Drive, Honolulu, HI 96822, USA

[2]European Southern Observatory, Alonso de Cordova 3107, Vitacura, Casilla 19001, Santiago, Chile

[3]Institute for Astronomy, The University of Edinburgh, Royal Observatory, Blackford Hill, Edinburgh EH9 3HJ, UK

[4]Gemini Observatory, Southern Operations Center, c/o AURA, Casilla 603, La Serena, Chile

[5]Steward Observatory, University of Arizona, 933 North Cherry Avenue, Tucson, AZ 85721, USA

[6]Goddard Space Flight Center, Code 667, Greenbelt, MD 20771, USA

[7]Mauna Kea Infrared, LLC, 21 Pookela St., Hilo, HI 96720, USA

1. Introduction

β Pic is a young ($\sim$12–21 Myr, Zuckerman et al. 2001; Binks & Jeffries 2014), nearby (19.44 pc, van Leeuwen 2007) A6 star that hosts one of the most prominent known debris disks (e.g. Smith & Terrile 1984; Wahhaj et al. 2003; Weinberger et al. 2003; Golimowski et al. 2006; Lagrange et al. 2012a). The disk midplane is warped, with a 4° offset between the inner warped disk and the outer main disk, suggesting a giant planet influencing the disk (Mouillet et al. 1997). This planet β Pic b was first detected in data from 2003, and the planet reappeared on the other side of the star in 2009 (Lagrange et al. 2009, 2010). β Pic b is one of the first planets to be directly imaged and has the smallest projected physical separation of any imaged planet to date. With a projected separation of $\sim$0.4" and a contrast of 9 magnitudes at K_S-band, the planet is challenging to detect even with state-of-the-art adaptive optics.

Orbital properties of directly imaged planets can encode clues to their formation. The eccentricities of these planets, for example, may trace migration or planet-planet interactions. β Pic b represents the longest-period exoplanet whose full orbital parameters can be determined with present observations. The estimated orbital period of $\sim$20 years allows us the opportunity to determine the orbit of this planet, whereas most other directly imaged planets will require many more decades of observations for a robust orbit determination. The orbital parameters of β Pic b are of particular interest since they allow us to study the relationship between the planet and the debris disk.

The Gemini NICI Planet-Finding Campaign was a 4-year survey to detect extrasolar planets conducted between 2008 and 2012 (Liu et al. 2010; Nielsen et al. 2013; Wahhaj et al. 2013b; Biller et al. 2013). In addition to detecting a number of brown dwarf companions (Biller et al. 2010; Wahhaj et al. 2011; Nielsen et al. 2012), we detected the planet β Pic b at multiple epochs over the course of the Campaign. We combine these observations with new data from Magellan MagAO and previous published work to determine the orbit of the planet.

2. Observations

VLT/NACO: Chauvin et al. (2012) present 9 epochs of β Pic b astrometry from VLT NACO, between 2003 and 2011. Bonnefoy et al. (2013) present an additional epoch from January 2012, as well as an improved orbital fit. We use the 10 astrometric observations and errors as reported in these works.

Gemini-South/NICI: We observed β Pic b with NICI at Gemini-South at 4 epochs between 2009 and 2012 (Table 1). Reductions were performed with the Gemini NICI Planet-Finding Campaign pipeline, described in depth in Wahhaj et al. (2013a). These data are discussed in detail in Males et al. (2014), which also includes a comparison to an independent analysis of some of the data by Boccaletti et al. (2013). We find that for overlapping epochs there is good agreement between

the NICI and NACO astrometry, indicating that there is no significant astrometric offset between the two instruments. In addition, NICI measurements have smaller uncertainties compared to those from NACO: the median separation and PA uncertainties are 0.005" and 0.6° for NICI and 0.011" and 1.81° for NACO. This increased precision is due to the partially transparent focal plane mask of NICI, which allows for an accurate measurement of the location of the star relative to the planet. Bonnefoy et al. (2013) note the primary source of error in their astrometry is the uncertainty in the position of the star.

Magellan/MagAO: β Pic b was observed on UT 2012 December 04 in the Y_S (0.985 μm) filter of Magellan MagAO+VisAO, and on UT 2012 December 01, 02, 04, and 07 in the 3.1 μm, 3.3 μm, L', and M' filters of Magellan MagAO+Clio2. The astrometry and photometry from MagAO+VisAO is described in detail in Males et al. (2014) and from MagAO+Clio2 in Morzinkski et al. (2014). The VisAO astrometry calibration is tied to the wider FOV Clio2 camera, and the two cameras are mounted simultaneously on the same rotator so they will have some common systematics, but the observations of the planet by these two cameras are otherwise independent measurements. Similar to NICI, the Magellan MagAO+VisAO instrument has a partially transmissive focal plane mask so the primary star is unsaturated in the data. MagAO+Clio2 data in 3.1 μm, 3.3 μm, and L' were taken with long and short exposures of saturated and unsaturated data, while M' data were entirely short unsaturated exposures.

3. MCMC Orbital Fitting

3.1. Methods

We use a Metropolis-Hastings Markov Chain Monte Carlo approach to fit orbital parameters to the astrometric motion of β Pic b from 2003 to 2012, following the procedure of Ford (2005) and Ford (2006). We compute two types of fits: one with the total system mass fixed (as done by all previous published orbital fits) and another with the total mass as a free parameter. For the fixed-mass case, we have six free parameters: the semi-major axis (a), eccentricity (e), inclination angle (i), argument of periastron (ω), position angle of nodes (Ω), and the epoch of periastron passage (T_0). The period (P) is determined from the semi-major axis using Kepler's Third Law and adopting a total system mass of 1.75 $M_\odot$ (Crifo et al. 1997). For the floating-mass fit, the orbital period is the seventh free parameter, so the total mass is allowed to take on any value.

At the start of the chain, initial values are chosen for each free parameter. A proposed trial step is taken by choosing a displacement in all parameters by randomly drawing from six (or seven) Gaussians centered on the current parameters with fixed standard deviations. The probability ratio between current and proposed orbit parameters is computed by determining the difference in the χ^2 statistic ($\Delta\chi^2$) for all astrometric epochs for β Pic b between the initial and trial sets of parameters. The choice of whether to adopt the trial parameters as the new step or to retain the current set is made via the Metropolis Hastings algorithm with probability ratio $\propto e^{\frac{-\Delta\chi^2}{2}}$.

Non-physical parameters ($a \leq 0$, $P \leq 0$, $e < 0$, $e \geq 1$) are assigned a χ^2 of 10^6 while the three viewing angles (i, ω, Ω) and epoch of periastron passage (T_0) are allowed to take any values without limits. To ensure the chains run efficiently, the standard deviations of the Gaussians for choosing trial steps are chosen initially via an iterative procedure where chains are run with different values of standard deviation for each parameter. The standard deviations corresponding to an acceptance rate of 0.44 are used for the final chains (Ford 2005).

After we terminate the MCMC chain, the angles are then wrapped around between 0° and 180° for inclination angle, -180° and 180° for argument of periastron, and 0° and 360° for position angle of nodes. Epoch of periastron passage is wrapped around to give a value in the range [2005,2005+period]. Without radial velocity measurements of the star's reflex motion there is an ambiguity between Ω and $\Omega + 180°$ — that is, whether the south-eastern half of the orbit is closer to the Earth or the north-western half — so while our chains only explored parameter space near Ω=212°, the results are equally valid for Ω=32°.[1]

Ten chains are run from the same starting parameters so that we may test for convergence using the Gelman-Rubin (GR) statistic, with 10^8 steps per chain and parameters saved every 1000 steps. The GR statistic is essentially the ratio of the variance in each parameter in individual chains to the total variance for all chains. If each chain is sampling the same region of parameter space then the GR metric will be very close to unity. If the chains are still exploring different regions of parameter space when the chains are terminated, then the GR statistic will be significantly larger than 1. A GR statistic less than 1.1 indicates the chains are converging, while less than 1.01 means excellent convergence (Ford 2006).

3.2. Results

We present medians and confidence intervals for each parameter in the fixed-mass case in Table 2. The inclination angle, argument of periastron, position angle of nodes, and epoch of periastron passage have a GR statistic less than 1.01, and the other two parameters have a GR statistic less than 1.1, indicating that our posterior distributions for all parameters are reliable.

Figure 1 displays the resulting marginalized posterior probability distributions for the orbital parameters and total system mass for both the fixed-mass and floating-mass cases. Figure 2 shows an example set of orbital parameters from the fixed-mass MCMC chains that has the lowest χ^2 within the 68% confidence region for all parameters (χ^2_ν=1.38).

[1]Lagrange et al. (2012b) present HARPS radial velocity data of β Pic between 2003 and 2010. The RV induced by the activity of the star dominates the expected reflex motion: the measured RV varies between −1.0 and 0.66 km/s with a standard deviation of 0.28 km/s, while the expected RV variation between 2003 and 2011 for the reflex motion of a 10 M_{Jup} planet with the median orbital parameters from the MCMC fit is 0.13 km/s. The linear fit to the RV computed by Lagrange et al. (2012b) indicates an increasing RV between 2003 and 2010, consistent with Ω near 212.

Our results for the fixed-mass case show an orbit with semi-major axis of about 9 AU is favored, with inclination angle and position angle of nodes (the two angles that describe the orientation of the orbit on the sky) very tightly constrained and eccentricity mainly <0.2. Figure 3 shows covariances between some orbital parameters for the fixed-mass fit. There is a strong correlation between eccentricity and semi-major axis, with larger values of semi-major axis corresponding to more eccentric orbits. Given the presence of the disk, it is unlikely that the orbit of the planet is significantly non-circular ($e \gtrsim 0.2$), and we expect future observations to be most consistent with the shorter-period circular orbits from our MCMC chain. With a uniform prior on eccentricity, we find $e < 0.15$ at 68% confidence and $e < 0.83$ at 95% confidence. If we were to impose a prior that eccentricity must be smaller than 0.2, we would obtain a=$8.9^{+0.8}_{-0.4}$ AU and P=$20.2^{+2.8}_{-1.2}$ yr, with the distributions for the other parameters about the same as in the uniform prior case. Our MCMC results find a median of time of maximum elongation (when the projected star-planet separation reaches a maximum) of 2012.63 and 68% (95%) confidence interval between 2012.56 (2012.49) and 2012.70 (2012.79). Our Magellan epochs are after turn around time in 99% of all orbits. So while the Magellan data represent the largest separation between star and planet in our astrometric record, our orbit fitting results indicate that maximum elongation was reached prior to these data being taken.

Finally, we consider the floating-mass MCMC fit. Though generally less constrained than the fixed-mass fit, the posterior mass distribution (lower right panel of Figure 1) shows that the previous estimated mass of 1.75 $M_\odot$ is well within the 68% confidence interval. While additional astrometry is required to place a more precise limit on the mass of the star β Pic, this total mass distribution of 1.7±0.3 $M_\odot$ indicates that our orbital fit and existing astrometric measurements are reasonable. Semi-major axis and period are highly correlated in our floating-mass fit, and while the chains have not converged for semi-major axis and period individually (GR statistics of 2), the GR statistic for mass is 1.0056, indicating a reliable measurement of the mass. If we were to impose the prior that $e < 0.2$ in the floating-mass case, our mass constraints for β Pic would slightly tighten to 1.7±0.2 $M_\odot$.

3.3. Comparison to Previous Fits

We now compare our results to previously published MCMC orbital fits. Comparing our posteriors to the results from Chauvin et al. (2012), we have similar distributions for semi-major axis and eccentricity but tighter constraints on the viewing angles of the orbit. For inclination angle and position angle of nodes, we find 88.9±0.7° and 211.8±0.3° compared to 88.5±1.7° and 212.6±1.5° from Chauvin et al. We find similar distributions in semi-major axis and eccentricity, though with smoother posteriors indicating our MCMC chains are better converged. (Chauvin et al. do not provide GR values for their fit but state that their GR statistics are consistent with convergence.) Since the preferred orbits from our chains are close to circular (68% having eccentricity less than 0.15), the argument of periastron and epoch of periastron passage are poorly

defined as they were for Chauvin et al., since it is difficult to determine periastron in a near-circular orbit. Nevertheless, the two values are tightly correlated (bottom right panel of Figure 3). While the location of periastron is not well-defined, the location of the planet at a particular epoch between ∼2000 and ∼2020 is.

Bonnefoy et al. (2013) refit the orbit with data from Chauvin et al. (2012) as well as an additional VLT data point from 2012 and find similar results, with MCMC chains that appear more converged than those of Chauvin et al. (2012). The semi-major axis from this fit is reported to be within 8–10 AU at 80% confidence; we find a less constrained semi-major axis, with 80% confidence lying between 8 and 14 AU. We also find a wider range of eccentricities that fit the data, with 80% confidence $e < 0.35$ compared to $e < 0.15$ reported by Bonnefoy et al. (2013). Conversely, we find tighter constraints on the orientation of the orbit on the sky. From their Figure 8, we determine that their inclination angle distribution is centered on 88.7° with a FWHM of 3.5°, and their distribution for position angle of nodes is centered on 212° and FWHM of 2.7°. Our distributions for these parameters have similar centers of 88.9° and 211.8°, but with smaller FWHMs of 1.7° and 0.7°.

4. Disk-Planet Alignment

In order to compare the position angle of the orbit to the disk, we perform a custom reduction of our 2011 NICI data to recover the disk. We begin by removing the azimuthally averaged profile of the point spread function from the individual images, as described in Wahhaj et al. (2013a) except that the running azimuthal average used here is taken over 90 pixels instead of 30 pixels. This process removes large scale (>90 pixels or 1.62") azimuthal structure from both the stellar halo and the disk. Since the β Pic disk is known to be edge-on, this procedure does not alter the disk profile significantly. After this step the disk reduction then proceeds with our standard ADI pipeline.

The signal-to-noise maps of the reduced images for the CH_4L and K_{cont} filters are shown in Figure 4. We consider only the flux from 80–120 AU separation in the reduced images to calculate the disk PA, following Lagrange et al. (2012a). The North-East (NE) and the South-West (SW) extensions of the disk were considered separately. We sum the pixel intensities between 80 and 120 AU along different PAs in steps of 0.1°, using cubic interpolation to estimate values at sub-pixel coordinates. These radial sums along the different PAs are then cubed, so that they can be used as weights. Only the radial sums that are one standard deviation or more above the rest are used. The disk PA is calculated as the weighted sum of the PAs within 20° of the NE and SW spines of the disk. We estimate a PA of 29.1±0.3° for the NE spine and 209.8±0.3° for the SW spine, in good agreement (within 1 and 2σ, respectively) with the first cADI 2-component fit values from Lagrange et al. (2012a) of $29.07^{\circ}{}^{+0.20}_{-0.19}$ and $209.00^{\circ}{}^{+0.16}_{-0.15}$

Using the Lagrange et al. (2012a) value of the position angle of the SW disk of $209.00^{\circ}{}^{+0.16}_{-0.15}$,

our measurement of the position angle of nodes of the orbit of 211.8±0.3° is 6σ discrepant with the position angle of the outer disk. The inner warped disk has a position angle of $212.9°^{+0.8}_{-0.3}$, which is discrepant at the 1.8σ level. Currie et al. (2011) presented a preliminary orbit based on four astrometric points and a non-MCMC method and found the position angle of nodes to be between the two disks. When we apply our MCMC method to their data we find generally larger uncertainties in orbital parameters than Currie et al. (2011) report. Using an MCMC fit to their data, we find the position angle of nodes to be 210.9±0.9°, 1.8σ greater than the outer disk PA and 1.7σ less than the inner disk PA. Chauvin et al. (2012) and Bonnefoy et al. (2013) fit more data with a similar MCMC method to ours and find the orbital plane of the planet to be consistent with the inner disk (Ω=212.6±1.5° and Ω=212.0±1.1°, respectively, both within 1σ of the PA of the inner disk of $212.9°^{+0.8}_{-0.3}$). By including our higher precision astrometric data and longer time baseline, we find the position angle of nodes to be between the two disks, though closer to the inner disk.

5. Discussion

We consider the implications of a misalignment between β Pic b and the two disks. Our observations recall a dynamical picture of the β Pic disk recently painted by Dawson et al. (2011). If a planet on an inclined orbit (inclination i_p) is introduced into a disk of non-interacting particles with zero initial inclination, the secular theory of Laplace-Lagrange (e.g. Murray & Dermott 1999) show us that the inclinations of the particles will oscillate about i_p, creating a cuspy disk structure with apparent inclination $2i_p$ in its inner regions. Our measurement that the planet's inclination is intermediate between the two observed disk planes seems to supports this picture. In contrast, earlier simulations by Mouillet et al. (1997) and Augereau et al. (2001) yielded a disk coplanar with the planet.

One important assumption built into the Dawson et al. (2011) model and supported by our observations is that the planetesimals are not yet collisionally relaxed, as models of structure in other debris disks have assumed (e.g. Quillen 2006, Rodigas et al. 2014). Another important assumption built into the Dawson et al. (2011) model is that the planet is introduced instantaneously, fully formed, at time zero. We infer that the β Pic disk is probably not collisionally relaxed; this inference should yield some interesting constraints on models of the collisional evolution of planetesimals in debris disks (e.g. Nesvold et al. 2013). Moreover, if the Dawson et al. (2011) model is indeed correct, it appears that the β Pic planet was introduced to its current orbit suddenly compared to the secular time scale, perhaps scattered there by another planet.

This notion begs us to ponder the role of multiple planets in sculpting the disk. In the context of their model, Dawson et al. (2011) placed severe limits on the presence of a second planet in the system disturbing the disk. In addition, Absil et al. (2013) exclude a second planet more massive than ∼5 M_{Jup} outside of 0.2" based on L' high contrast images of β Pic. But what caused the inclination of β Pic b if not an interaction with another massive planet? And how did the

planetesimals respond to this interaction? These questions remain unanswered.

Finally, we consider the transit event noted by Lecavelier Des Etangs et al. (1995) in November 1981 and find very loose constraints on a transit of the planet given the available data. We search for such a transit by finding the smallest projected distance between star and planet between 2003 and 2008 and then subtract one orbital period from the returned epoch for each step in our MCMC chains. We find the most recent closest approach to be at epoch $2007.44^{+0.13}_{-0.17}$. The median value for the epoch of closest approach one orbital period earlier is 1986.5, with a 68% confidence interval between 1951.9 and 1988.3 (95% confidence between 1542.3 and 1989.7, given the long tail of the posterior for orbital period). The smallest projected distance from star to planet is less than 29 times the radius of β Pic (1.8 ± 0.2 $R_\odot$); Di Folco et al. 2004) at 68% confidence (<47 times the radius at 95% confidence). Thus we cannot rule out a transit with the current orbital fit. Lecavelier Des Etangs et al. (1995) and Chauvin et al. (2012) speculate that the transit event may not be caused by the planet itself but rather by solid material entrained by the planet and carried in its Hill sphere. We cannot rule out this possibility either, and more data are required. Radial velocity measurements of the star are required to determine if this most recent closest approach corresponds to a transit or occultation. If we again adopt the linear fit of Lagrange et al. (2012b) to the HARPS RV data for β Pic then the planet would be passing in front of the star in 2007, as well as in 1981. We predict that the next occultation will take place between 2017.41 and 2018.38 at 68% confidence (2017.26–2019.37 at 95% confidence), with a median epoch of 2017.59. Additional astrometric observations in the next few years will provide a more precise occultation window and occultation probability.

6. Conclusions

We have examined the orbit of β Pic b given five new epochs of data taken with Gemini/NICI and Magellan/MagAO, finding a semi-major axis of $9.2^{+8.3}_{-0.5}$ AU and a period of 21^{+34}_{-2} years. The astrometric record of β Pic b is now long enough to be able to remove the assumption of a particular system mass, which was needed by all previous fits to this orbit. When we solve for the mass of β Pic itself we find a value of 1.7 ± 0.3 $M_\odot$, consistent with the expected value of 1.75 $M_\odot$. The position angle of nodes for our fixed-mass orbit is offset (1.8σ) from the observed position angle of the inner warped disk and 6σ discrepant with the position angle of the outer disk, suggesting that the disk is not collisionally relaxed.

Our orbital fit indicates that the planet has reached maximum elongation and is currently moving back toward the star, crossing to the other side of the star by ≈2018. β Pic b has been observed extensively since its reappearance in 2009 and this window for studying the planet will remain open for just a few more years before the planet is undetectable behind the star again. Advanced planet-finding instruments such as GPI and SPHERE will likely allow for orbital monitoring of the planet closer to the star, so the time of lost contact is likely to be significantly shorter than it was between 2003 and 2009.

We thank Jessica Lu and Adam Kraus for helpful discussions. B.A.B was in part supported by Hubble Fellowship grant HST-HF-01204.01-A awarded by the Space Telescope Science Institute, which is operated by AURA for NASA under contract NAS 5-26555. This work was supported in part by NSF grants AST-0713881 and AST-0709484 awarded to M. Liu. The Gemini Observatory is operated by the Association of Universities for Research in Astronomy, Inc., under a cooperative agreement with the NSF on behalf of the Gemini partnership: the National Science Foundation (United States), the Science and Technology Facilities Council (United Kingdom), the National Research Council (Canada), CONICYT (Chile), the Australian Research Council (Australia), CNPq (Brazil), and CONICET (Argentina). This research has made use of the SIMBAD database, operated at CDS, Strasbourg, France.

Facilities: Gemini:South (NICI), Magellan II (MagAO+Clio2), Magellan II (MagAO+VisAO).

REFERENCES

Absil, O., Milli, J., Mawet, D., Lagrange, A.-M., Girard, J., Chauvin, G., Boccaletti, A., Delacroix, C., & Surdej, J. 2013, A&A, 559, L12

Augereau, J. C., Nelson, R. P., Lagrange, A. M., Papaloizou, J. C. B., & Mouillet, D. 2001, A&A, 370, 447

Biller, B. A., Liu, M. C., Wahhaj, Z., Nielsen, E. L., Close, L. M., Dupuy, T. J., Hayward, T. L., Burrows, A., Chun, M., Ftaclas, C., Clarke, F., Hartung, M., Males, J., Reid, I. N., Shkolnik, E. L., Skemer, A., Tecza, M., Thatte, N., Alencar, S. H. P., Artymowicz, P., Boss, A., de Gouveia Dal Pino, E., Gregorio-Hetem, J., Ida, S., Kuchner, M. J., Lin, D., & Toomey, D. 2010, ApJ, 720, L82

Biller, B. A., Liu, M. C., Wahhaj, Z., Nielsen, E. L., Hayward, T. L., Males, J. R., Skemer, A., Close, L. M., Chun, M., Ftaclas, C., Clarke, F., Thatte, N., Shkolnik, E. L., Reid, I. N., Hartung, M., Boss, A., Lin, D., Alencar, S. H. P., de Gouveia Dal Pino, E., Gregorio-Hetem, J., & Toomey, D. 2013, ApJ, 777, 160

Binks, A. S. & Jeffries, R. D. 2014, MNRAS, 438, L11

Boccaletti, A., Lagrange, A.-M., Bonnefoy, M., Galicher, R., & Chauvin, G. 2013, A&A, 551, L14

Bonnefoy, M., Boccaletti, A., Lagrange, A.-M., Allard, F., Mordasini, C., Beust, H., Chauvin, G., Girard, J. H. V., Homeier, D., Apai, D., Lacour, S., & Rouan, D. 2013, A&A, 555, A107

Chauvin, G., Lagrange, A.-M., Beust, H., Bonnefoy, M., Boccaletti, A., Apai, D., Allard, F., Ehrenreich, D., Girard, J. H. V., Mouillet, D., & Rouan, D. 2012, A&A, 542, A41

Crifo, F., Vidal-Madjar, A., Lallement, R., Ferlet, R., & Gerbaldi, M. 1997, A&A, 320, L29

Currie, T., Thalmann, C., Matsumura, S., Madhusudhan, N., Burrows, A., & Kuchner, M. 2011, ApJ, 736, L33

Dawson, R. I., Murray-Clay, R. A., & Fabrycky, D. C. 2011, ApJ, 743, L17

Di Folco, E., Thévenin, F., Kervella, P., Domiciano de Souza, A., Coudé du Foresto, V., Ségransan, D., & Morel, P. 2004, A&A, 426, 601

Ford, E. B. 2005, AJ, 129, 1706

—. 2006, ApJ, 642, 505

Golimowski, D. A., Ardila, D. R., Krist, J. E., Clampin, M., Ford, H. C., Illingworth, G. D., Bartko, F., Benítez, N., Blakeslee, J. P., Bouwens, R. J., Bradley, L. D., Broadhurst, T. J., Brown, R. A., Burrows, C. J., Cheng, E. S., Cross, N. J. G., Demarco, R., Feldman, P. D., Franx, M., Goto, T., Gronwall, C., Hartig, G. F., Holden, B. P., Homeier, N. L., Infante, L., Jee, M. J., Kimble, R. A., Lesser, M. P., Martel, A. R., Mei, S., Menanteau, F., Meurer, G. R., Miley, G. K., Motta, V., Postman, M., Rosati, P., Sirianni, M., Sparks, W. B., Tran, H. D., Tsvetanov, Z. I., White, R. L., Zheng, W., & Zirm, A. W. 2006, AJ, 131, 3109

Lagrange, A.-M., Boccaletti, A., Milli, J., Chauvin, G., Bonnefoy, M., Mouillet, D., Augereau, J. C., Girard, J. H., Lacour, S., & Apai, D. 2012a, A&A, 542, A40

Lagrange, A.-M., Bonnefoy, M., Chauvin, G., Apai, D., Ehrenreich, D., Boccaletti, A., Gratadour, D., Rouan, D., Mouillet, D., Lacour, S., & Kasper, M. 2010, Science, 329, 57

Lagrange, A.-M., De Bondt, K., Meunier, N., Sterzik, M., Beust, H., & Galland, F. 2012b, A&A, 542, A18

Lagrange, A.-M., Gratadour, D., Chauvin, G., Fusco, T., Ehrenreich, D., Mouillet, D., Rousset, G., Rouan, D., Allard, F., Gendron, É., Charton, J., Mugnier, L., Rabou, P., Montri, J., & Lacombe, F. 2009, A&A, 493, L21

Lecavelier Des Etangs, A., Deleuil, M., Vidal-Madjar, A., Ferlet, R., Nitschelm, C., Nicolet, B., & Lagrange-Henri, A. M. 1995, A&A, 299, 557

Liu, M. C., Wahhaj, Z., Biller, B. A., Nielsen, E. L., Chun, M., Close, L. M., Ftaclas, C., Hartung, M., Hayward, T. L., Clarke, F., Reid, I. N., Shkolnik, E. L., Tecza, M., Thatte, N., Alencar, S., Artymowicz, P., Boss, A., Burrows, A., de Gouveia Dal Pino, E., Gregorio-Hetem, J., Ida, S., Kuchner, M. J., Lin, D., & Toomey, D. 2010, in Society of Photo-Optical Instrumentation Engineers (SPIE) Conference Series, Vol. 7736, Society of Photo-Optical Instrumentation Engineers (SPIE) Conference Series

Males, J. R., Close, L. C., Morzinkski, K. M., Wahhaj, Z., Liu, M. C., et al. 2014, submitted ApJ

Morzinkski, K. M., Close, L. C., Males, J. R., et al. 2014, in prep. ApJ

Mouillet, D., Larwood, J. D., Papaloizou, J. C. B., & Lagrange, A. M. 1997, MNRAS, 292, 896

Murray, C. D. & Dermott, S. F. 1999, Solar system dynamics

Nesvold, E. R., Kuchner, M. J., Rein, H., & Pan, M. 2013, ApJ, 777, 144

Nielsen, E. L., Liu, M. C., Wahhaj, Z., Biller, B. A., Hayward, T. L., Boss, A., Bowler, B., Kraus, A., Shkolnik, E. L., Tecza, M., Chun, M., Clarke, F., Close, L. M., Ftaclas, C., Hartung, M., Males, J. R., Reid, I. N., Skemer, A. J., Alencar, S. H. P., Burrows, A., de Gouveia Dal Pino, E., Gregorio-Hetem, J., Kuchner, M., Thatte, N., & Toomey, D. W. 2012, ApJ, 750, 53

Nielsen, E. L., Liu, M. C., Wahhaj, Z., Biller, B. A., Hayward, T. L., Close, L. M., Males, J. R., Skemer, A. J., Chun, M., Ftaclas, C., Alencar, S. H. P., Artymowicz, P., Boss, A., Clarke, F., de Gouveia Dal Pino, E., Gregorio-Hetem, J., Hartung, M., Ida, S., Kuchner, M., Lin, D. N. C., Reid, I. N., Shkolnik, E. L., Tecza, M., Thatte, N., & Toomey, D. W. 2013, ApJ, 776, 4

Quillen, A. C. 2006, MNRAS, 372, L14

Rodigas, T. J., Malhotra, R., & Hinz, P. M. 2014, ApJ, 780, 65

Smith, B. A. & Terrile, R. J. 1984, Science, 226, 1421

van Leeuwen, F. 2007, A&A, 474, 653

Wahhaj, Z., Koerner, D. W., Ressler, M. E., Werner, M. W., Backman, D. E., & Sargent, A. I. 2003, ApJ, 584, L27

Wahhaj, Z., Liu, M. C., Biller, B. A., Clarke, F., Nielsen, E. L., Close, L. M., Hayward, T. L., Mamajek, E. E., Cushing, M., Dupuy, T., Tecza, M., Thatte, N., Chun, M., Ftaclas, C., Hartung, M., Reid, I. N., Shkolnik, E. L., Alencar, S. H. P., Artymowicz, P., Boss, A., de Gouveia Dal Pino, E., Gregorio-Hetem, J., Ida, S., Kuchner, M., Lin, D. N. C., & Toomey, D. W. 2011, ApJ, 729, 139

Wahhaj, Z., Liu, M. C., Biller, B. A., Nielsen, E. L., Close, L. M., Hayward, T. L., Hartung, M., Chun, M., Ftaclas, C., & Toomey, D. W. 2013a, ApJ, 779, 80

Wahhaj, Z., Liu, M. C., Nielsen, E. L., Biller, B. A., Hayward, T. L., Close, L. M., Males, J. R., Skemer, A., Ftaclas, C., Chun, M., Thatte, N., Tecza, M., Shkolnik, E. L., Kuchner, M., Reid, I. N., de Gouveia Dal Pino, E. M., Alencar, S. H. P., Gregorio-Hetem, J., Boss, A., Lin, D. N. C., & Toomey, D. W. 2013b, ApJ, 773, 179

Weinberger, A. J., Becklin, E. E., & Zuckerman, B. 2003, ApJ, 584, L33

Zuckerman, B., Song, I., Bessell, M. S., & Webb, R. A. 2001, ApJ, 562, L87

This preprint was prepared with the AAS LaTeX macros v5.2.

Table 1. New Astrometry for β Pic b

Instrument	Filter	Sep. (“)	PA(°)	Epoch (UT)
Gemini/NICI	CH_4S (4%)	0.323±0.010	209.3±1.8	2009 Dec 03
Gemini/NICI	CH_4L (4%)	0.339±0.010	209.2±1.7	2009 Dec 03
Gemini/NICI	K_S	0.407±0.005	212.9±1.4	2010 Dec 25
Gemini/NICI	CH_4S (1%)	0.455±0.003	211.9±0.4	2011 Oct 20
Gemini/NICI	K_{cont}	0.452±0.005	211.6±0.6	2011 Oct 20
Gemini/NICI	CH_4S (1%)	0.447±0.003	210.8±0.4	2012 Mar 29
Gemini/NICI	K_{cont}	0.448±0.005	211.8±0.6	2012 Mar 29
Magellan/MagAO+Clio2	3.1 μm, 3.3μm, L', M'	0.461±0.014	211.9±1.2	2012 Dec 02
Magellan/MagAO+VisAO	Y_S	0.470±0.010	212.0±1.2	2012 Dec 04

Table 2. Orbital Parameters of β Pic b

Parameter	Lowest χ^2	Median	68% CI	95% CI	GR Stat.
Fixed Mass					
Semi-major Axis (AU)	9.3	9.2	8.7–17.5	8.2–72.3	1.0478
Eccentricity	0.05	0.08	0.02–0.50	0.00–0.88	1.0438
Inclination Angle (°)	88.9	88.9	88.2–89.6	87.4–90.4	1.0008
Argument of Periastron (°)	14.3	-8	-90–98	-168–168	1.0011
Position Angle of Nodes (°)	211.8	211.8	211.5–212.1	211.2–212.4	1.0015
Epoch of Periastron Passage	2013.32	2012	2010–2019	2006–2023	1.0033
Period (yr)	21.41	21	19–55	18–465	...
Floating Mass					
Semi-major Axis (AU)	121.7	27.0	9.0–98.9	8.4–121.6	1.9751
Eccentricity	0.93	0.68	0.10–0.91	0.01–0.93	1.4140
Inclination Angle (°)	89.1	89.0	88.4–89.7	87.6–90.3	1.0064
Argument of Periastron (°)	347.6	-15	-35–8	-130–143	1.0025
Position Angle of Nodes (°)	211.6	211.7	211.4–211.9	211.2–212.3	1.0236
Epoch of Periastron Passage	2011.52	2011	2010–2013	2007–2021	1.0164
Period (yr)	1019.50	110	21–775	18–1054	2.0327
Mass ($M_\odot$)	1.74	1.65	1.37–1.96	1.12–2.39	1.0056

Note. — Results from the MCMC fit to the orbit of β Pic b and orbital parameters for the lowest χ^2 within the 68% confidence interval from the chains (Figure 2).

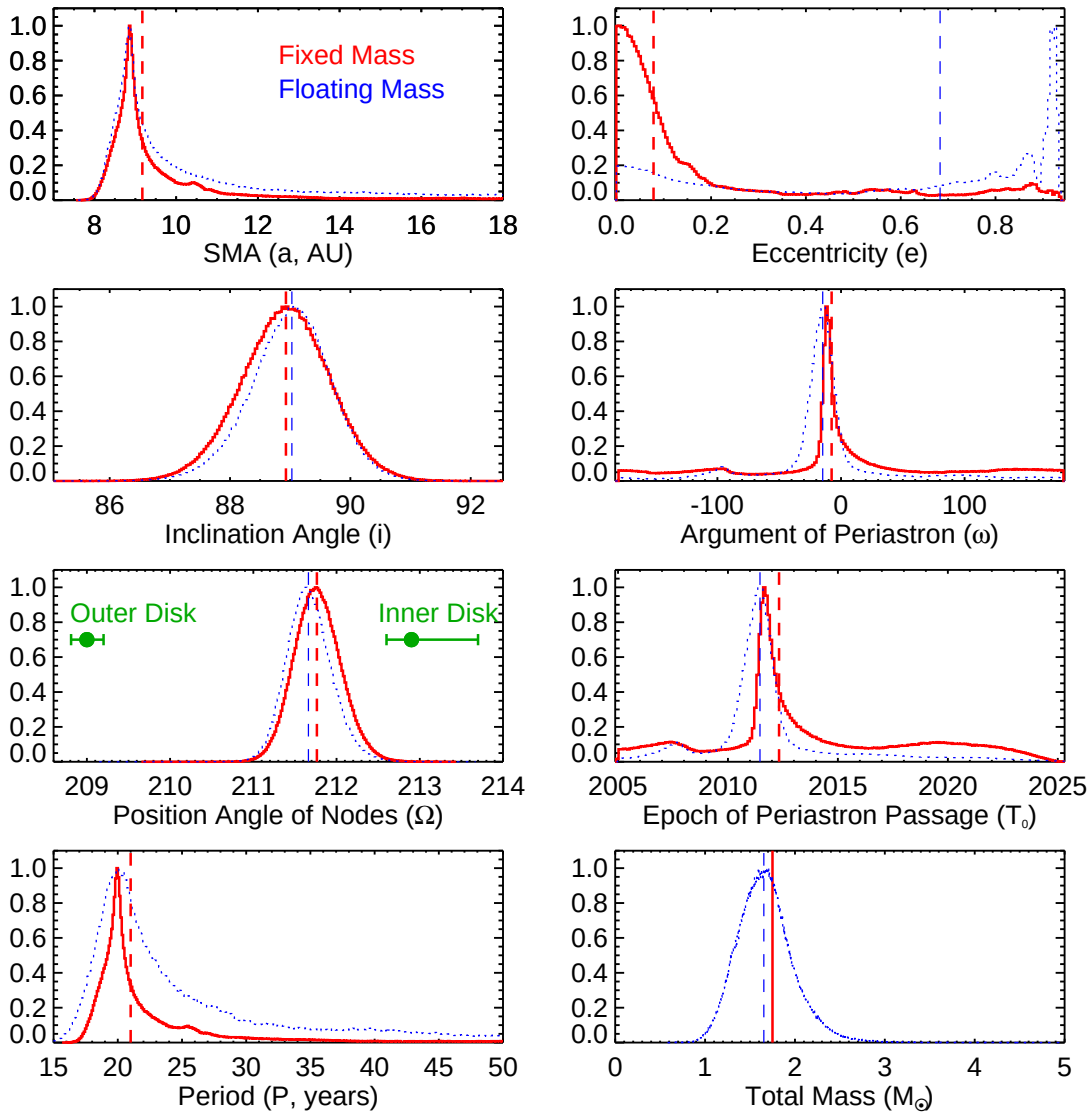

Fig. 1.— Marginalized distributions of orbital parameters from our MCMC fit to the orbit of β Pic b, for the cases where the total mass of the system is fixed at 1.75 $M_{\odot}$ (red solid lines) and floating as a free parameter (blue dotted lines). The distributions have been normalized so that their peaks are unity. Dashed lines mark the median of each distribution, and green points and error bars denote the position angle of the outer main and inner disk as measured by Lagrange et al. (2012a).

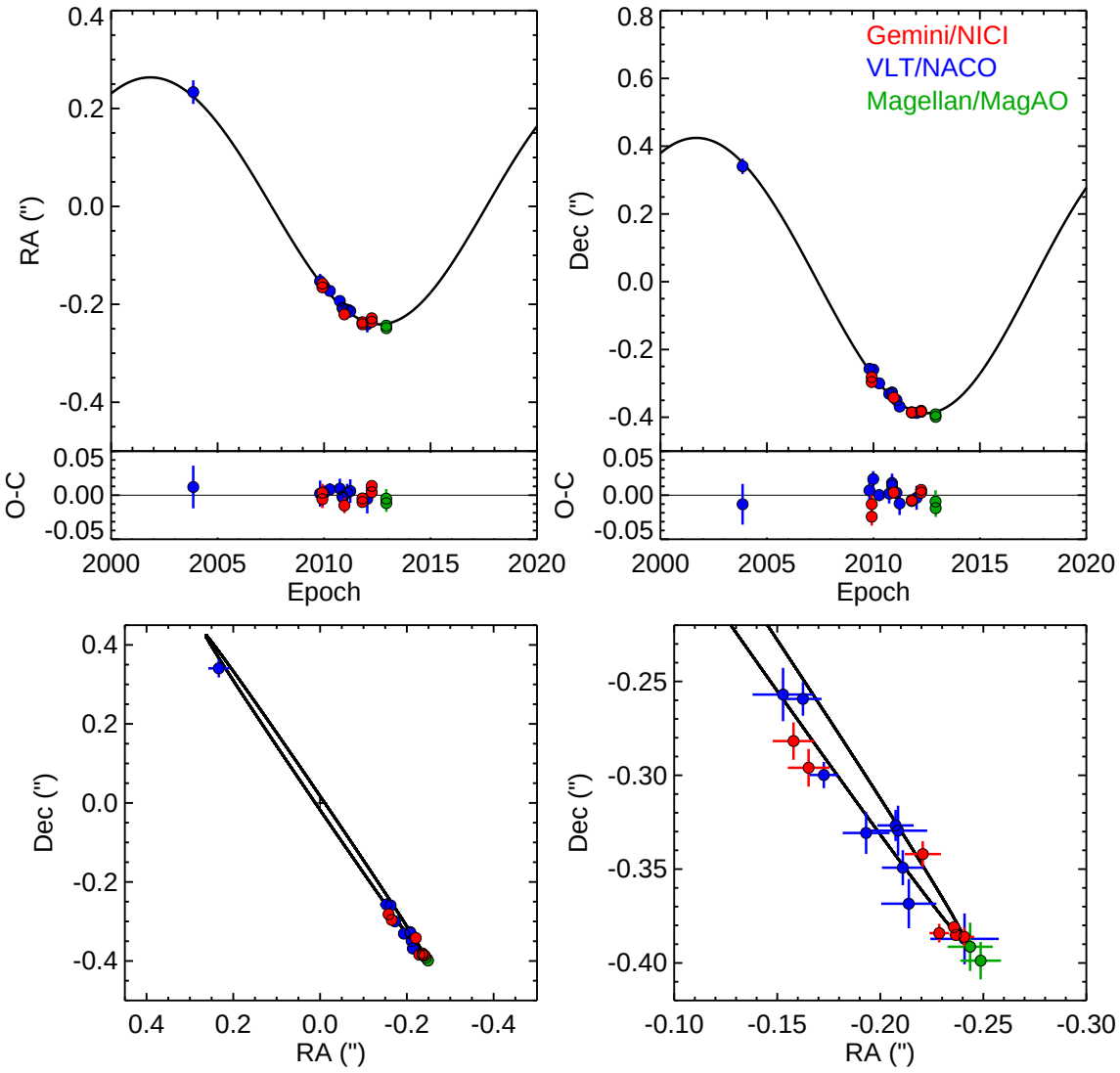

Fig. 2.— The lowest χ^2 orbit within the 68% confidence interval from our fixed-mass MCMC chain, and residuals plotted as Observed - Calculated (O-C), corresponding to a χ^2_ν=1.38 for 31 degrees of freedom.

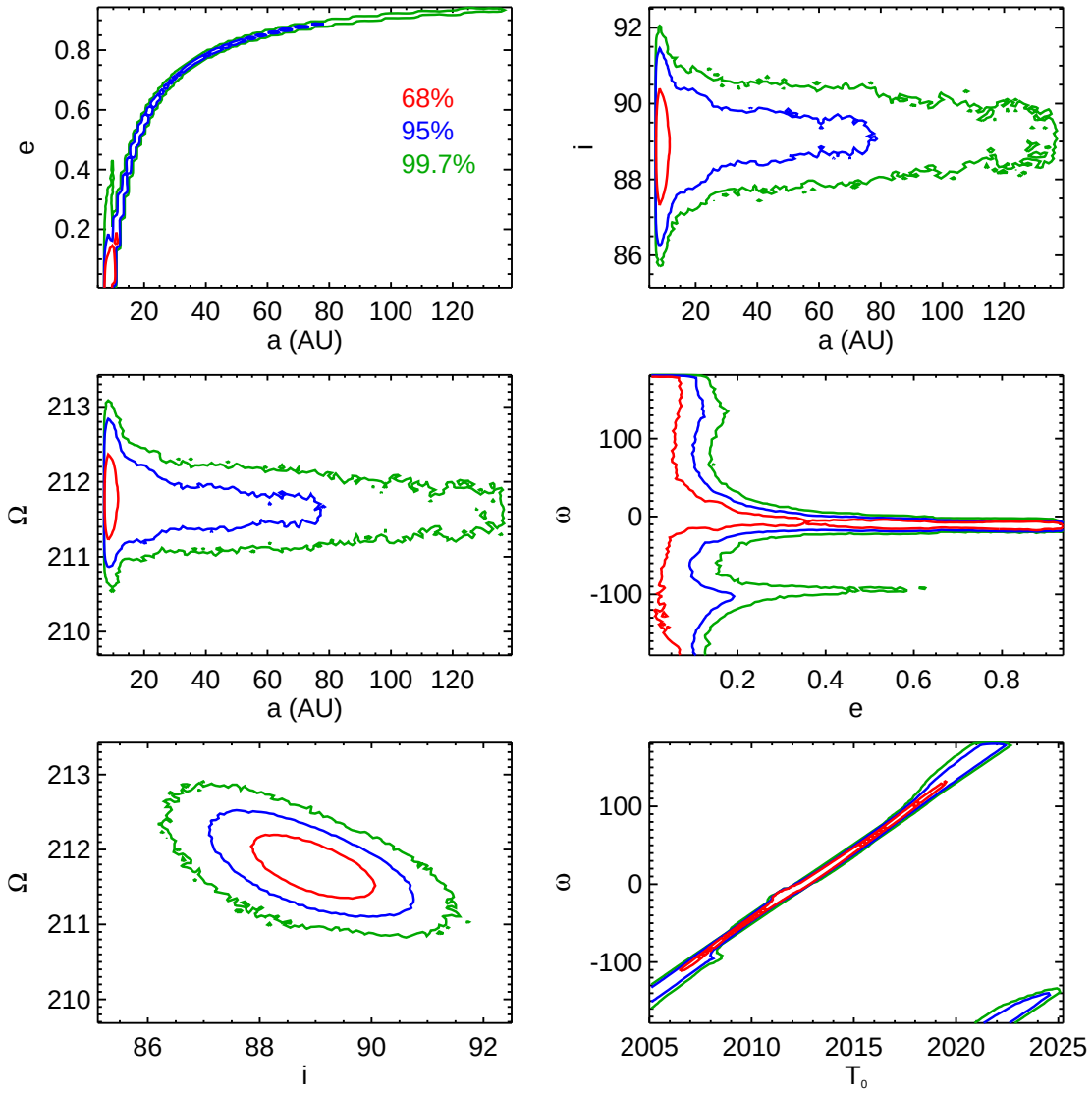

Fig. 3.— Covariances between parameters (semi-major axis a, eccentricity e, inclination angle i, argument of periastron ω, position angle of nodes Ω, and epoch of periastron passage T_0) for the MCMC orbital fit with total mass fixed to 1.75 $M_\odot$. Lower semi-major axis corresponds to lower eccentricity, with the most probable orbits close to circular with small semi-major axis. The position angle of nodes and inclination angle are tightly constrained and correlated, with position angle of nodes 1.8σ from the PA inner disk and 6σ from the PA of the outer disk.

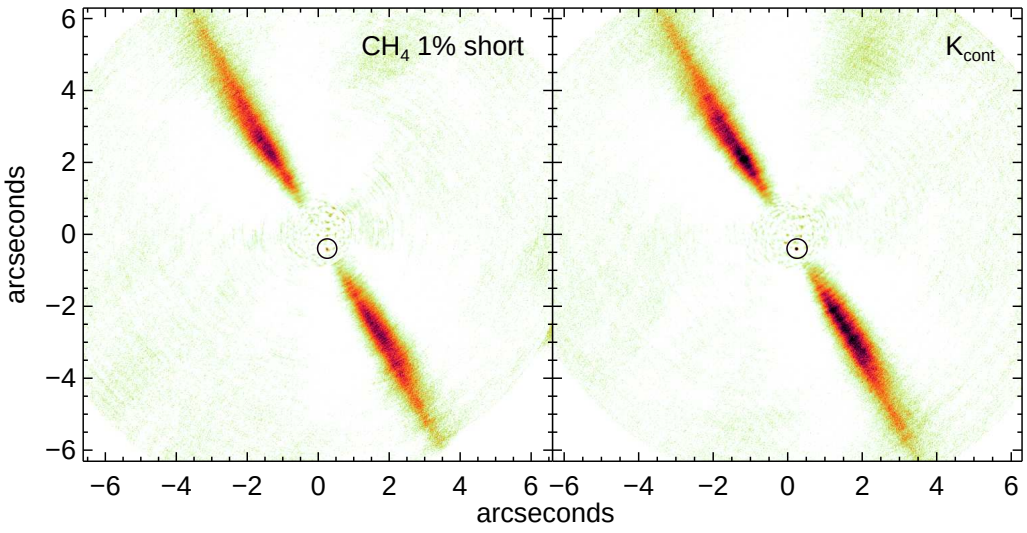

Fig. 4.— Signal-to-noise maps of our Gemini NICI observations of β Pic from 2011 showing both disk and planet in CH_4S (left) and K_{cont} (right). The figure is oriented with North up and East to the left. The black circle marks the location of the planet.